

Generation of CO and Smoke During Underventilated Combustion

S. LÉONARD, G. W. MULHOLLAND,* R. PURI, and R. J. SANTORO

Department of Mechanical Engineering, The Pennsylvania State University, University Park, PA 16802

The CO and smoke yields observed for underventilated laminar diffusion flames are presented for methane and ethene for global equivalence ratio Φ over the range 0.5 to 4.0. A Burke–Schumann type burner with fuel in the center tube and air in the annular region was used. The peak CO yields for methane and ethene, 0.37 and 0.47, respectively, are at least a factor of 100 greater than for overventilated burning. The ratio of CO/CO₂ versus Φ for the methane flame is compared with local measurements of this ratio for both overventilated and underventilated laminar diffusion flames and with the results for turbulent natural gas flames quenched in an upper layer. The peak smoke yields for methane at a flow rate of 10 cm³/s and for ethene at a fuel flow rate of 6.4 cm³/s are 0.01 and 0.05, respectively, compared with yields of 0.0 and 0.028 for the overventilated case. The proportionality between smoke yield and CO yield observed for overventilated burning for a wide range of fuels is found not to be valid for the underventilated case. The chemical makeup and structure of the smoke produced at high equivalence ratio is qualitatively different from smoke produced under overventilated conditions; the smoke is mainly organic rather than graphitic and it has an agglutinated structure rather than an agglomerate structure with distinct primary spheres usually observed in overventilated burning.

INTRODUCTION

While there has been extensive research on overventilated laminar diffusion flames in terms of smoking height, yield of smoke and combustion gases, and species concentrations in the flame itself, there has been relatively little research on underventilated laminar diffusion flames beyond the work of Burke and Schumann [1]. Studies recently have been conducted of inverse laminar diffusion flames [2, 3], which represent a closely related flame configuration. In these studies the oxidizer flow is surrounded by the fuel flow; the reverse of the normal laminar diffusion flame arrangement. There have been several studies of the species produced by underventilated turbulent flames [4–11]. These include small scale studies of CO yield for slightly underventilated burning for solid fuels [4] and for propane and propylene [5]. In larger-scale tests [6–11] with turbulent flames the overall ventilation is controlled by adjusting the height of the collection

hood relative to the burner. The fuels studied include methane by Toner et al. [6, 8], methane, ethene, and propylene by Morehart et al. [7, 9] and a variety of hydrocarbons, alcohols, as well as several polymers by Beyler [10, 11]. In these studies there is an abrupt increase in the CO concentration as the global equivalence ratio, Φ , defined as the fuel-to-air ratio normalized by the stoichiometric fuel-to-air ratio approaches a value of 1.0. This large increase in CO is of concern in regard to safety implications for fires in structures and continuing research is under way to characterize the CO production during underventilated burning in enclosures [12, 13].

The focus of the present study is to provide a quantitative data base on the production of CO and smoke particulates from laminar underventilated diffusion flames à la Burke Schumann [1]. Advantages of the underventilated laminar diffusion flame system over previous studies [4–13] include a wider range of Φ up to at least 4, the ease in measuring Φ and the yields of CO and smoke, and the potential for theoretical analysis of the generation rates of the combustion products. We have chosen to study methane, which is the simplest hydrocar-

*National Institute of Standards and Technology, Gaithersburg, MD 20899.

bon, and ethene, which has a moderate tendency to smoke. Methane [14–17] and ethene [18–21] are among the most carefully studied fuels for laminar overventilated flames. There are also data [6–9] for CO concentration on turbulent underventilated flames for these gases. We are not aware of any quantitative study of smoke production during underventilated burning.

In the present study emphasis is given to the general trends observed for both CO and soot production in terms of the global equivalence ratio. The trends in the CO and soot yields in these underventilated laminar flame studies differ distinctively from results observed in overventilated diffusion flames. Additionally the very nature of the soot formed in these flames is different from that observed in the more widely studied overventilated conditions. Care is also taken to describe the conditions under which stable underventilated flames can be established and the procedure for systematically observing the effects of the equivalence ratio variations.

EXPERIMENT

A Burke–Schumann type burner [1] with fuel in the center and air in the annular region (Fig. 1) was used in this study. In the Burke–Schumann study, the diameters of two concentric tubes were selected so that the air and fuel velocities were matched. If we were to maintain this condition in our study, a separate burner would be required for each value of Φ . Instead, we have used primarily two burner configurations. This simplifies the measurements and still allows us to assess the effect of the mismatch in the air and fuel velocities on the yield of CO and smoke. We have found that the qualitative trends in regard to the yield of CO and smoke as a function of Φ are insensitive to the velocity effect and, thus, focus this paper on a single burner configuration. Selected results are presented for a second burner configuration.

For overventilated ethene flames, there is an abrupt transition from non-smoking to smoking with a small change in fuel flow rate. For this reason, we have performed yield measurements for ethene flow rates corresponding to a

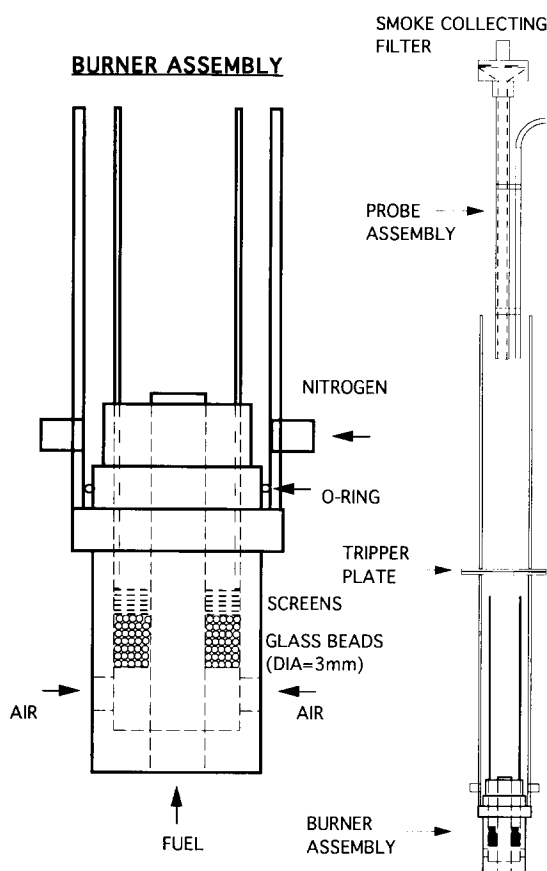


Fig. 1. Illustration of burner, dilution system, and probe assembly.

nonsmoking flame and to a smoking flame. While this produced a larger effect than changing the burner configuration, it still did not affect the qualitative trends. We focus our discussion on a single flow rate of $6.4 \text{ cm}^3/\text{s}$ for ethene, which corresponds to a smoking flame for overventilated burning, and a flow rate of $10 \text{ cm}^3/\text{s}$ for methane. Selected results for a second flow rate of ethene are included.

Burner / Diluter Design

The burner design parameters and burner conditions are contained in Fig. 1 and Table 1. Most of the results presented in this article relate to configuration 1. The burner housings were machined from 50.8 mm (2 in) and 25.4 mm (1 in) diameter brass. It was convenient to use nominal 9.6 mm (3/8 in) and 12.7 mm (1/2 in) brass tubing for the fuel tubes. The

TABLE 1
Tube Dimensions for Coflow Burners

	Inner Tube (mm) ^a	Outer Tube (mm) ^b
Burner configuration 1	9.6 o.d. (3/8 in) 7.3 i.d.	29 I.D. 32 o.d.
Burner configuration 2	9.6 o.d. (3/8 in) 7.3 i.d.	22 I.D. 25 o.d.
Burner configuration 3	12.7 o.d. (1/2 in) 11.2 i.d.	22 I.D. 25 o.d.

^aBrass.

^bQuartz.

lengths of the fuel tubes, about 20 cm, were chosen to be long enough to ensure well developed laminar flow at the outlet. The height of the fuel tube can be adjusted by loosening a compression fitting which is screwed into the base of the burner. Either burner tube (inner tube) could be attached to each of the two burner housings.

The air flow enters the base of the annular region, flows through a 2-cm layer of 3-mm-diameter glass beads, and then through six layers of 70-gauge screen to provide laminar air flow. The inner glass tube (quartz) fits against the top of the screen located about 6 cm below the fuel tube. This quartz tube is sealed to the outer brass surface with a tape made from polytetrafluoroethylene (PTFE). The use of quartz enables one to burn off smoke deposits between experiments with a non-smoking methane flame as the outer surface is heated with a propane torch.

The outer glass tube, which serves as a concentric dilution tube, is sealed to the outer burner tube with a rubber stopper for the smaller burner housing and with an O-ring fitted for the larger housing. The two dilution tubes were fitted with polished flanges to minimize leaks and to facilitate assembly. The purpose of the dilution tube is to provide uniform mixing of the smoke and gases and to cool the smoke particulate prior to collection with minimal deposition on the walls. The dominant mechanism of smoke particulate deposition in this system is via thermophoresis, which is proportional to the temperature gradient near the wall. Cooling by rapid dilution by N₂ reduces the temperature gradient and consequently the

particle deposition relative to cooling by only heat exchange with the walls of the tube.

The nominal N₂ flow rate is 590 cm³/s (35.4 L/min), which dilutes the combustion product by a factor of 2 to a factor of 30 depending on the combustion air flow rate. The combustion products mix with the N₂ as they pass through a tripper plate. Visual observation of scattered light from a laser beam passing through the diluted combustion products indicated that for a 50.8-mm (2-in) diameter tube a tripper plate with a 19.1-mm (3/4-in) orifice provided good mixing at a dilution flow rate of 590 cm³/s (35.4 L/min). The gas and smoke sampling position was located approximately 5 tube diameters downstream of the orifice. Subsequent gas sampling at seven uniformly spaced radial positions indicated a radial variation of less than 2% for both CO and CO₂. Variations in repeated measurements over the time period required for the radial profile were comparable to the apparent radial variation.

Two rotameters with overlapping ranges were used for the fuel flow and two for air flow to allow accurate flow rate monitoring over the range 2 to 20 cm³/s for fuel and 10 to 280 cm³/s for the air. Each flow meter was calibrated to an accuracy of about ±2% using soap film flow meters with volumes of 1.0 and 2.5 L and a dry test meter with a 10-L displacement. A nitrogen flow meter and filter collection critical orifice were also calibrated with the dry test meter. Precautions were taken to select the proper tubing size to minimize the pressure drop between the outlet of the flow meter and the burner.

Gas Analysis

The gas and particulate sampling systems are illustrated in Fig. 2. Both sampling inlets are

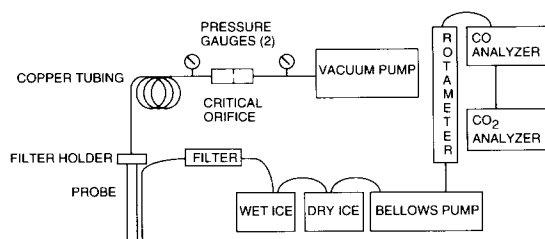


Fig. 2. Illustration of sampling and analysis system.

Laminar Diffusion Flames

— Predicted Flame Height (All Dimensions in mm)

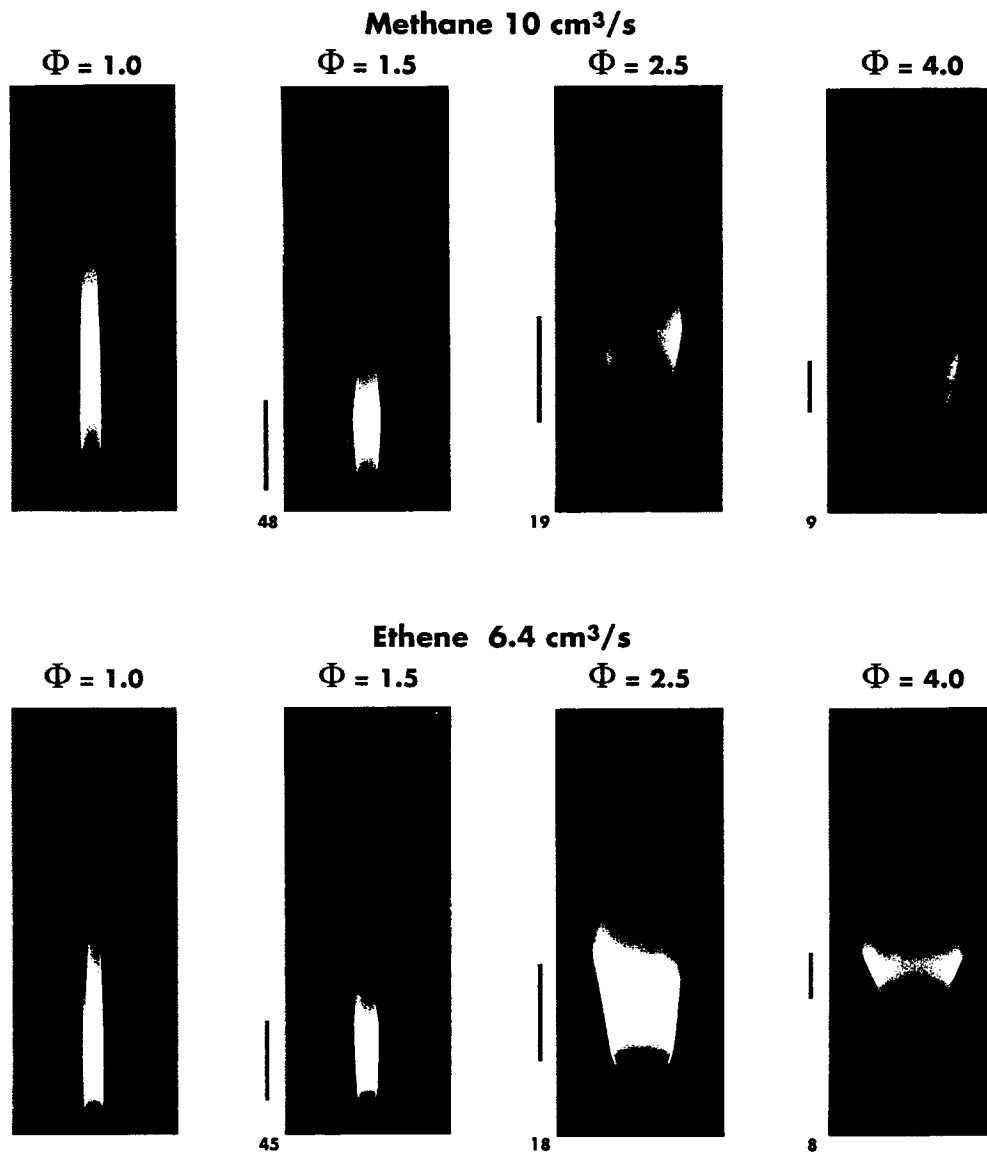


Fig. 3. Flame photographs of methane at a fuel flow rate of 10 cm³/s and ethene at a fuel flow rate of 6.4 cm³/s versus ϕ for burner configuration 1. The solid lines adjacent to the pictures for $\phi > 1.0$ represent the predicted flame height in mm from the Burke Schumann theory.

located about 2.5 cm below the end of the dilution tube, which is covered with a screen. The gas sampling system consisted of a 6.5-mm (1/4-in) diameter tube about 250 mm in length to provide some cooling before passing through a high capacity pleated filter. The gases then flow through a 1-m length of 9.5-mm (3/8-in) diameter copper tubing in a wet ice bath followed by about a 1.2-m length of tubing surrounded by dry ice (see Fig. 2). There was a drain cap in the wet ice bath to remove condensate. The flow then went through a displacement pump at a flow rate of about 13.3 cm³/s (0.8 L/min) followed by a NDIR CO analyzer and a NDIR CO₂ analyzer.

Standard calibration procedures were used with the gas analyzers involving zeroing the meters with dry N₂ and then spanning with standard Reference Material Gas Mixtures (NIST SRM 2619a, 5066 ± 5 ppm CO₂ in N₂; NIST SRM 2637a, 2400 ± 24 ppm CO in N₂). The sensitivity of the CO meter is 0.001% and for the CO₂ meter is 0.01%. The measured values of CO during underventilated burning were in the range 0.07% to 0.5% while the CO₂ ranged from about 0.2% to 2%. The drift in the zero was on the order of the instrument sensitivity. A slight cross sensitivity of the CO meter to ethene was observed. For example, for a flow rate of 6.4 cm³/s of ethene and 590 cm³/s (35.4 L/min) of N₂ the CO reading increased 0.002% under noncombusting conditions. Since the ethene concentration would be reduced greatly under flame conditions the cross sensitivity introduces a negligible error in the results. The estimated uncertainty in the CO gas analyzer is ±2% of the reading over the range of 0.15% to 0.5% and in the CO₂ gas analyzer is ±3% of the reading over the range of 0.3% to 1.0%.

Our system afforded 3–4 h of continuous operation before requiring thawing of the line going through the dry ice bath. In a typical measurement sequence, we would record readings for the CO and CO₂ gas analyzers, change Φ by changing the air flow rate, and, after about a 60-s equilibration time, record the gas analyzer readings for the new condition. The detailed characterization of the CO and CO₂ for a given fuel involved 13 values of Φ equally

spaced on a logarithmic scale between 0.5 and 4 and required about 1 h to complete.

Smoke Particulate Analysis

The smoke sampling system consisted of a 15.9-mm (5/8-in) o.d. steel sampling tube 360 mm long, a 4.7-mm-diameter filter holder, 3 m of 9.5-mm (3/8-in) diameter copper tubing, a critical orifice to control the flow rate, and a vacuum pump (see Fig. 2). The smoke sampling tube provided cooling of the gases from an inlet gas temperature of 200°C for the 10 cm³/s methane flame burning at $\Phi = 0.5$ to a temperature of about 100°C at the filter holder. For the other flame conditions, both the inlet and filter gas temperatures were lower. The cooling prevented deterioration of the polytetrafluoroethylene (PTFE) coated filter. The collection efficiency for the filter (Pallflex¹ T60A20) is reported [22] to be 70 to 80% for 0.035- μ m-diameter particles and at least 95% for particles with diameter of 0.3 μ m and larger. The 3-m length of copper tubing assured that the gas temperature was at ambient conditions at the orifice. The vacuum pump operated at 1/10 of ambient pressure assuring a choked flow. The nominal flow rate through the filter was 153 cm³/s (9.2 L/min). The flow rate was measured each day by attaching a dry test meter to the inlet of the smoke sampling system. Pressure gauges were attached for monitoring both the vacuum pressure and the pressure drop across the filter. The maximum pressure drop across the filter was 1.3 kPa (50-in water) during the filter collection and this corresponded to about 15 mg of smoke collected on the filter.

Smoke collection required about 5 min, after which the filter was removed and replaced with another preweighed filter. Typically one filter sample was collected for each of five different values of Φ during one set of measurements.

¹Certain commercial equipment, instruments, and materials are identified in order to adequately specify the experimental procedure. Such identification does not imply recommendation by the National Institute of Standards and Technology, nor does it imply that the materials identified are necessarily the best for the purpose.

The mass of smoke collected on the filter varied from about 0.1 mg to about 15 mg and in most cases exceeded 1 mg. Our filter weighings were repeatable to ± 0.02 mg using a microbalance with a 0.01 mg sensitivity.

An estimate was made of the amount of smoke deposited on the tube walls relative to the amount collected on the filter. The smoke on the wall of the combustion tube was collected with a tissue attached to a plunger device. A second plunger arrangement was used for the dilution tube. Smoke was also collected from the orifice plate and the smoke sampling tube. The dilution tube accounted for most of the smoke deposition. Repeat measurements gave smoke depositions of 12% and 14%. These deposition measurements were made for the case of a relatively high gas temperature of 170°C, so we expect this estimate to provide an upperbound.

Filter samples were also collected at very light loadings on quartz fiber filters for analysis of the organic and elemental carbon fraction of the smoke versus Φ . This was done by a contract laboratory using thermo-optical analysis for organic/elemental carbon [23]. The "organic" and "elemental" carbon are determined by a two-step pyrolysis, the first using helium as the carrier gas at 720°C and the second with 5% oxygen in helium at 720°C. The "organic" carbon is obtained from the total carbon produced during the first step and the "elemental" carbon is determined from the second step. Smoke samples were collected for transmission electron microscopy on 3-mm-diameter copper grids coated with a thin carbon layer. The grids were attached to a metal surface with double stick tape and held over the dilution tube exit for a period of 1–100 s depending on the smoke concentration.

FLAME STRUCTURE

Changing the value of Φ for a fixed burner configuration resulted in a mismatch in the air and fuel velocity. This differed from the Burke–Schumann study, where the air and fuel flows were typically matched. We obtained stable flames for all conditions except the low flow rate ethene flame (3.2 cm³/s) for burner

configuration 1. In this case, an oscillation of the flame at about 1 Hz first occurs for $\Phi = 1.52$. This corresponds to an air velocity equal to 2/3 of the fuel velocity. The oscillations become more pronounced as Φ is increased above 1.52. Other qualitative features include the flame front bending below the burner for an ethene fuel flow rate of 3.2 cm³/s, $\Phi = 4$ for burner configuration 1 and flame blowoff for methane at a fuel flow rate of 20 cm³/s, $\Phi = 0.7$ with burner configurations 2 and 3, which have the smaller diameter outer tube.

The effect of Φ on flame shape for the methane and ethene flames is illustrated in Fig. 3 (see color plate facing page 34). For $\Phi = 4$ the flame front is clearly curving toward the outer tube, though such a curvature is not clearly evident at $\Phi = 1.5$. There does appear to be a slight necking in for $\Phi = 1.5$, and this may signify the termination of the outward flame zone. A similar observation regarding the "central bright part of the flame rising above the actual flame" was made by Burke and Schumann in their original study [1]. The necking in of the luminous region observed in the present study is not attributed to the location of the reaction front, but rather to the transport of incandescent smoke particles. The actual reaction front should proceed to the wall as required for underventilated conditions [1]. The fact that the flame front does not extend to the wall of the burner makes the determination of a precise flame height difficult. Thus, we have taken the flame height for underventilated flames to correspond to the location where the flame begins to neck in. This location nearly corresponds to the end of the bright yellow region observed in the flames shown in Fig. 3.

In Fig. 3, we have also included the predicted flame height (the solid line adjacent to the picture) based on Burke–Schumann theory using a diffusion coefficient of 0.60 cm²/s, which corresponds to the diffusion coefficient of oxygen at 575 K. Roper [24] found that his data for circular port flames could be fit to the Burke–Schumann theory using this value of the diffusion coefficient. As previously pointed out, the Burke–Schumann theory assumes equal air and fuel exit velocities, which enter into the theory through the air and fuel tube

diameters. Since the exit velocities were not equal in the experiments, some adjustment had to be made to compare to the theory. For the present study the actual fuel tube inner diameter (7.3 mm) was used and an effective diameter for the outer air passage was calculated for use in the theory such that the air and fuel velocities were equal. The predicted flame height from the Burke–Schumann analysis is greater than the blue zone, but is clearly less than the maximum luminous height (see Fig. 3). The increase in flame height with decreasing Φ is qualitatively predicted by the Burke–Schumann theory. The flame shapes are qualitatively similar for both the methane and ethene flames, but the much more intense luminous radiation from the smoke in the flame is apparent for the ethene case. Long exposure times were required for the ethene flames to bring out the bluish reaction zone presumably arising from CH radicals.

CO AND SMOKE DATA ANALYSIS

The measured volume percent of CO and CO₂ in the diluted gases on a dry basis are plotted versus Φ in Fig. 4 for the methane flame at a fuel flow rate of 10 cm³/s and include a set of repeat measurements several weeks apart. An equal spacing of points on a logarithmic scale in Φ was used to provide both good coverage near the rapidly changing region around $\Phi = 1.0$ and coverage over the entire range from $\Phi = 0.5$ to $\Phi = 4.0$. We see from Table 2 that the volume percent for CO, X_{CO} , increases from 0.001 (the minimum detection limit for the CO analyzer) to 0.31 as Φ increases from 0.76 to 1.32. The 0.31% CO for the diluted combustion products corresponds to an estimated 2.5% CO prior to dilution with nitrogen. This estimate is based on the flow rates of nitrogen, methane, and air (Table 2). The degree of dilution increases with increasing Φ . For example, the estimated peak CO concentration prior to dilution with nitrogen is 2.9% at $\Phi = 2.0$.

It is convenient to express the results in terms of the yield, ϵ , on a mass basis, where ϵ_{CO} is equal to the mass of CO produced per mass of fuel entering the burner. The procedure for determining the yield is outlined be-

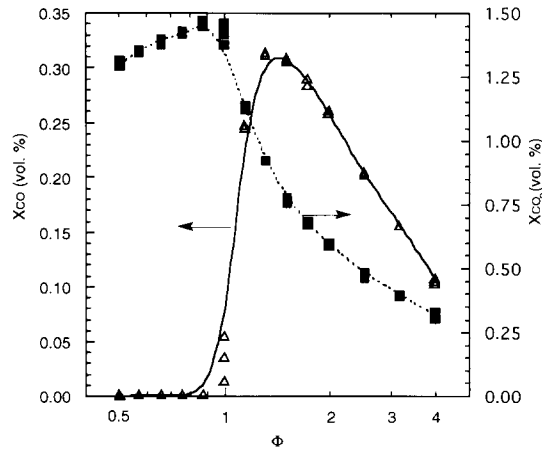


Fig. 4. Volume percent of CO and CO₂ versus log Φ for a methane flame with a fuel flow rate of 10 cm³/s (data from Table 2).

low. First the volume flow rate of CO, F_{CO} , is computed from the measured volume percent of CO, X_{CO} , and the total volumetric flow rate through the dilution tube, F_T , corrected to ambient conditions.

$$F_{CO} = \frac{X_{CO} F_T}{100}. \quad (1)$$

Next the density of CO, ρ_{CO} , is obtained from the ideal gas law as

$$\rho_{CO} = \frac{M_{CO} P_A}{RT_A}, \quad (2)$$

where M_{CO} is the molecular weight of CO and the subscript A refers to ambient conditions. From Eqs. 1 and 2 we obtain the total mass flow rate of CO, \dot{m}_{CO} , as

$$\dot{m}_{CO} = \frac{X_{CO} F_T}{100} \frac{M_{CO} P_A}{RT_A}. \quad (3)$$

To compute the yield of CO we also need the mass flow rate of fuel, which is obtained from the volumetric flow rate of the fuel, F_F , and its density, ρ_F . Using an expression similar to Eq. 2 for computing the density, we obtain the following expression for the mass flow rate of fuel:

$$\dot{m}_F = F_F \frac{M_F P_A}{RT_A}. \quad (4)$$

TABLE 2
Results for Burner Configuration 1 for Methane and Ethene

Methane: 10 cm ³ /s; Dilution: 590 cm ³ /s of N ₂									
Results for CO and CO ₂ Measurements									
Φ	Air Flow (cm ³ /s)	Total Flow (cm ³ /s)	X _{CO} (vol. %)	X _{CO₂} (vol. %)	Smoke (mg)	ε _{CO} (gCO/gCH ₄)	ε _{CO₂} (gCO ₂ /gCH ₄)	ε _s ^a (gC/gCH ₄)	Carbon Balance
0.50	190	790	0.001	1.32	—	0.001	2.87	—	1.04
0.57	166	766	0.001	1.36	—	0.001	2.87	—	1.04
0.66	144	744	0.001	1.40	—	0.001	2.87	—	1.04
0.76	126	726	0.001	1.44	—	0.001	2.86	—	1.04
0.87	109	709	0.001	1.48	—	0.001	2.88	—	1.05
1.00	95.2	695	0.013	1.47	—	0.016	2.80	—	1.03
1.15	82.8	683	0.245	1.14	—	0.293	2.14	—	0.95
1.32	72.2	672	0.311	0.93	—	0.366	1.72	—	0.83
1.52	62.8	663	0.308	0.78	—	0.357	1.42	—	0.72
1.74	54.7	655	0.284	0.69	—	0.325	1.23	—	0.63
2.00	47.7	648	0.258	0.60	—	0.292	1.07	—	0.56
2.52	37.8	638	0.203	0.49	—	0.227	0.85	—	0.44
3.18	30.0	630	0.156	0.40	—	0.172	0.69	—	0.35
4.00	23.8	624	0.105	0.33	—	0.115	0.56	—	0.27
Results for CO, CO ₂ , and Smoke Measurements									
0.50	190	790	0.0	1.30	0.0	0.0	2.82	0.0	1.03
1.00	95.2	695	0.055	1.38	4.29	0.067	2.64	0.010	1.01
1.52	62.8	663	0.305	0.76	4.68	0.354	1.38	0.009	0.72
2.52	37.8	638	0.205	0.46	0.79	0.229	0.81	0.0013	0.43
4.00	23.8	624	0.102	0.31	0.0	0.111	0.52	0.0	0.25
Ethene: 6.4 cm ³ /s; Dilution: 590 cm ³ /s of N ₂									
Results for CO and CO ₂ Measurements									
Φ	Air Flow (cm ³ /s)	Total Flow (cm ³ /s)	X _{CO} (vol. %)	X _{CO₂} (vol. %)	Smoke (mg)	ε _{CO} (gCO/gC ₂ H ₄)	ε _{CO₂} (gCO ₂ /gC ₂ H ₄)	ε _s ^b (gC/gC ₂ H ₄)	Carbon Balance
0.50	183	779	0.002	1.60	—	0.002	3.07	—	0.98
0.57	159	755	0.002	1.66	—	0.002	3.07	—	0.98
0.66	139	735	0.002	1.69	—	0.002	3.05	—	0.97
0.76	121	717	0.003	1.72	—	0.003	3.03	—	0.96
0.87	105	701	0.005	1.74	—	0.006	3.00	—	0.96
1.00	91.3	688	0.015	1.75	—	0.016	2.96	—	0.95
1.15	79.5	676	0.209	1.50	—	0.221	2.49	—	0.90
1.32	69.2	666	0.369	1.22	—	0.384	2.00	—	0.83
1.52	60.3	657	0.448	1.00	—	0.459	1.62	—	0.74
1.74	52.5	649	0.459	0.84	—	0.465	1.34	—	0.66
2.00	45.7	642	0.434	0.72	—	0.435	1.13	—	0.58
2.52	36.3	633	0.363	0.56	—	0.359	0.87	—	0.46
3.18	28.8	625	0.280	0.46	—	0.273	0.71	—	0.36
4.00	22.8	619	0.180	0.37	—	0.174	0.56	—	0.27
Results for CO, CO ₂ , and Smoke Measurements									
0.50	183	779	0.002	1.59	7.03	0.002	3.05	0.028	0.99
1.00	91.3	688	0.032	1.69	14.70	0.034	2.85	0.051	0.96
1.52	60.3	657	0.446	0.98	13.70	0.457	1.58	0.044	0.76
2.52	36.3	633	0.358	0.54	5.95	0.354	0.84	0.019	0.45
4.00	22.8	619	0.177	0.35	1.99	0.171	0.53	0.0037	0.26

^aSampling conditions correspond to laboratory temperature and pressure conditions: $T = 23^{\circ}\text{C}$ and $P = 731.7$ mmHg at a sample probe flow rate of 152 cm³/s.

^bSampling conditions correspond to laboratory temperature and pressure conditions: $T = 23^{\circ}\text{C}$ and $P = 736.4$ mmHg at a sample probe flow rate of 155 cm³/s.

The yield of CO, ϵ_{CO} , is obtained from Eqs. 3 and 4 as the ratio of the mass flow rate of CO to the mass flow rate of fuel.

$$\epsilon_{\text{CO}} = \frac{\dot{m}_{\text{CO}}}{\dot{m}_F} = \frac{X_{\text{CO}} F_T M_{\text{CO}}}{100 F_F M_F}. \quad (5)$$

The above expression requires that the fuel and combustion products are at, or are corrected to, the same temperature and pressure.

In Eq. 5, we approximate the total volumetric flow rate F_T as the sum of the volumetric flow rates of N_2 , fuel, and air. This is a good approximation since the volumetric flow rate of N_2 accounts for at least 94% of the inlet flow rate for both the methane flame at a flow rate of $10 \text{ cm}^3/\text{s}$ and the ethene flame at a flow rate of $6.4 \text{ cm}^3/\text{s}$ for all values of Φ measured for a typical dilution flow rate of N_2 of $590 \text{ cm}^3/\text{s}$ ($35.4 \text{ L}/\text{min}$). Furthermore, for both methane and ethene, the sum of the number of moles of CO_2 and H_2O produced by complete combustion is equal to the sum of the number of fuel and oxygen moles. For Φ less than or equal 1, complete combustion is a good approximation. This can be deduced from the results in Table 2. The ratio of the measured ϵ_{CO_2} to the predicted value based on complete combustion (2.75 for methane and 3.14 for ethene) differs at most 6% from 1.0. For $\Phi > 1$ there is a significant amount of CO and possibly H_2 produced in addition to H_2O and CO_2 ; however as Φ increases, an increasingly large percentage of the inlet flow is N_2 . For $\Phi = 1.5$, 97% of the inlet flow is N_2 for the two fuel flow rates given above. The production of smoke will result in a reduction in the outlet gas flow rate; however, even if 10% of the fuel carbon becomes smoke for ethene, which is greater than any value we measured, the reduction in the volumetric flow rate is only 0.1% for $\Phi = 1$.

So we see that for $\Phi > 1$, the above flow rate approximation is valid to within about 3%. One other factor plays a role for Φ in the range 0.5–1.0; that is, the fact that the water produced by the combustion is removed by the wet and dry ice traps. Assuming complete combustion and assuming all the water is removed by the cold traps, we find that the total flow rate is reduced by 2.9% for methane at 10

cm^3/s and 1.9% for ethene at $6.4 \text{ cm}^3/\text{s}$. We conclude that approximating F_T as the sum of the N_2 , air, and fuel flow rate is valid to within 3%. Below we provide a consistency check of this approximation.

The other quantity of interest is the smoke yield, ϵ_s , which is determined from the mass flow rate of smoke to the filter, \dot{m}_s , the mass flow rate of the fuel, \dot{m}_F , and the volumetric dilution factor, f_{dil} , which is equal to the ratio of F_T to the volumetric gas flow rate through the filter, F_f .

$$\epsilon_s = \frac{\dot{m}_s}{\dot{m}_F} f_{\text{dil}}. \quad (6)$$

The mass flow rate of the fuel is based on the fuel volumetric flow rate taking into account the laboratory temperature and pressure conditions.

Typical results for methane at a fuel flow rate of $10 \text{ cm}^3/\text{s}$ and ethene at $6.4 \text{ cm}^3/\text{s}$ are given in Table 2. We see that the repeat CO yield measurements for $\Phi \geq 1.52$ agree within 2%; the large difference at $\Phi = 1.0$ results from the great sensitivity of yield to Φ near $\Phi = 1$.

An estimate of the accuracy of our method for computing gaseous yields can be made by comparing measured CO_2 yield for $\Phi = 0.5$ with the predicted CO_2 yield for complete combustion for methane and ethene. For over-ventilated burning the major carbon-containing product of combustion is CO_2 . For methane at $\Phi = 0.5$, the measured yields are about 4% greater than the predicted value of 2.75, while for ethene the measured values are about 2% less than the predicted value of 3.14. From the CO_2 analogue of Eq. 5 we estimate an overall uncertainty of $\pm 6\%$ by combining the uncertainties associated with volume fraction and flow rate measurements. Thus, the methane and ethene results are within the expected uncertainty range. For ethene, 2%–3% of the fuel carbon is emitted as smoke particulate at $\Phi = 0.5$ so perfect agreement with the predicted value of 3.14 is not expected. In Table 2 a carbon balance is included as the ratio of the mass outflow of carbon based on CO_2 , CO, and smoke to mass inflow of carbon in the fuel. The repeatability of the CO yield measure-

ments is $\pm 3\%$ over the range $1.15 < \Phi < 4$ (see Table 2 and Fig. 5). Combining in quadrature the repeatability uncertainty with the systematic uncertainties in the CO gas analyzer, $\pm 2\%$, and the flow uncertainty, $\pm 3\%$, leads to a combined uncertainty of $\pm 5\%$ of the measured CO yield. At $\Phi = 0.5$, the uncertainty is on the order of $\pm 50\%$ because the CO concentration is so low as to approach the instrument noise.

The measured smoke yields are an underestimate by 20%–25% because of the estimated 13% wall deposition and a nominal 10% penetration of the smoke through the filter. The estimated repeatability of the smoke yield results, $\pm 8\%$, is more variable than for the CO yield, because one additional flow rate (smoke sampling flow) is needed and because of the variability associated with particle deposition and penetration.

CO AND SMOKE YIELD RESULTS

The CO yield increases abruptly with Φ to a peak value of 0.37 for methane and 0.47 for ethene. As shown in Fig. 5, the peak in the methane curve occurs at a slightly smaller Φ than for ethene, 1.3 relative to 1.7. The CO yield is very sensitive to small changes in Φ near $\Phi = 1$ and larger differences are obtained for repeat measurements near $\Phi = 1$.

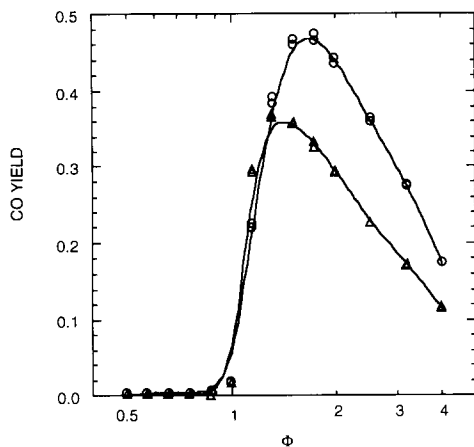


Fig. 5. Yield of CO for methane at a fuel flow rate of $10 \text{ cm}^3/\text{s}$ (Δ) and for ethene at a fuel flow rate of $6.4 \text{ cm}^3/\text{s}$ (\circ) versus Φ based on data in Table 2 and repeat measurements made on another day.

Additional measurements were performed at other fuel flow rates and with a second burner configuration to determine the generality of this shift and the results were inconclusive in regard to the difference being attributed to fuel chemistry. As indicated in Fig. 6, decreasing the fuel flow rate for ethene by a factor of 2 to $3.2 \text{ cm}^3/\text{s}$ shifts the peak to the left by an amount similar to the difference between ethene at $6.4 \text{ cm}^3/\text{s}$ and methane at $10 \text{ cm}^3/\text{s}$.

The smoke yield curve peaks at smaller Φ , near 1.0, compared with the result for CO yield as shown in Fig. 7. Also for large Φ , the percentage decrease for smoke is much greater than for CO. This will become more apparent when the results are presented in an alternative form in the discussion session. While the repeatability of the smoke yield measurements is not as good as that of CO and CO_2 yields, the results are consistent with our predicted repeatability of $\pm 8\%$. The same general curve shape was obtained with methane as ethene as shown in Fig. 8 though the ethene peak is about 5 times as great as the peak for methane.

The smoke yield decreases sharply for $\Phi > 1.5$ as shown in Fig. 9 as the fuel flow rate decreases. This is the same trend as for the CO yield (see Fig. 6). The large reduction in the smoke yield at $\Phi = 0.5$ for the $3.2 \text{ cm}^3/\text{s}$ fuel flow rate case is expected since the fuel flow rate is then below the smoke point for the overventilated flame.

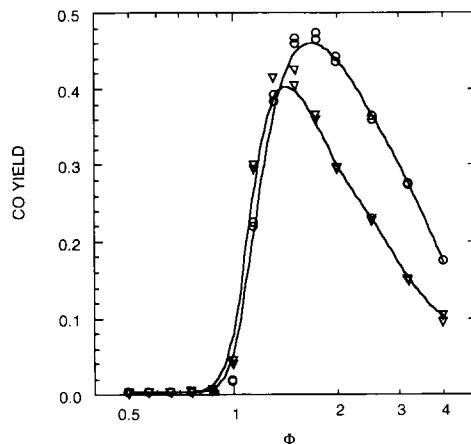


Fig. 6. Yield of CO for ethene at a fuel flow rate of $6.4 \text{ cm}^3/\text{s}$ (\circ) and a fuel flow rate of $3.2 \text{ cm}^3/\text{s}$ (∇) versus Φ .

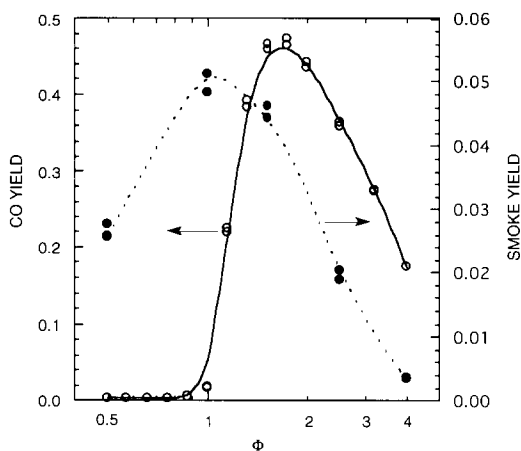


Fig. 7. Yields of CO (O) and smoke (●) as function of Φ for ethene at a fuel flow rate of $6.4 \text{ cm}^3/\text{s}$.

As discussed in the first section, we performed experiments on several burner configurations. Here we show results on two configurations. In the second configuration the quartz tube is smaller making the air velocity about a factor of two greater than in the first. The yields are qualitatively similar for the two burner configurations as shown in Fig. 10. Increasing the air velocity results in a slight increase in the CO yield but a slight decrease in the smoke yield. There is a surprising result at $\Phi = 0.5$ that the smoke yield goes to zero for the higher air velocity even though the fuel flow rate is well above the smoke point.

We noticed from the filter samples that the smoke generated at large Φ appeared lighter

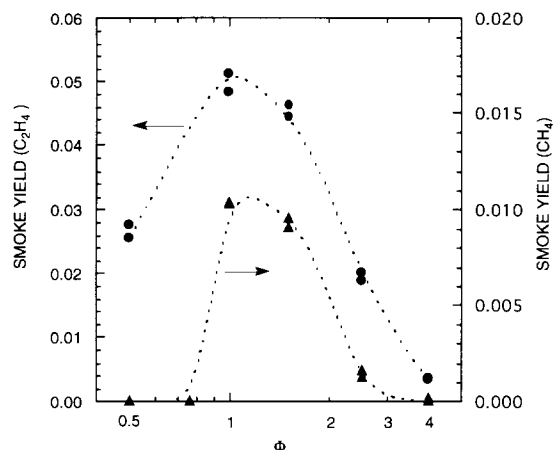


Fig. 8. Yield of smoke for ethene at a flow of $6.4 \text{ cm}^3/\text{s}$ (●) and for methane at a fuel flow rate of $10 \text{ cm}^3/\text{s}$ (▲).

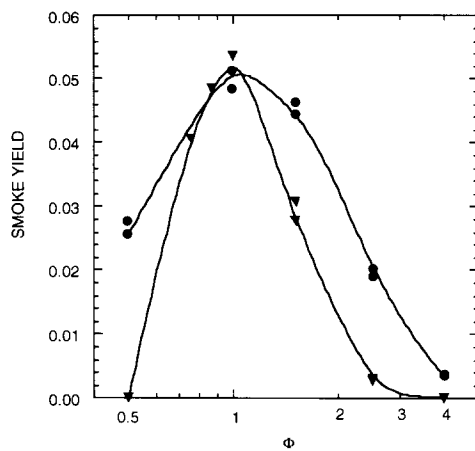


Fig. 9. Yield of smoke for ethene at a fuel flow rate of $6.4 \text{ cm}^3/\text{s}$ (●) and at a fuel flow rate of $3.2 \text{ cm}^3/\text{s}$ (▼).

in color and that the deposit on the combustion burner tube had a liquid character. In fact, for methane at $\Phi = 4$, the filter had a yellowish appearance. Thermo-optical analysis of the smoke collected on the quartz filters indicated that as Φ increased, the organic fraction of the smoke increased relative to the elemental carbon fraction. As indicated in Table 3, at $\Phi = 4$ for both fuels the organic fraction is greater than the elemental fraction. This is in sharp contrast to the results at $\Phi = 1$ and $\Phi = 0.5$, where less than 10% of the smoke is organic carbon.

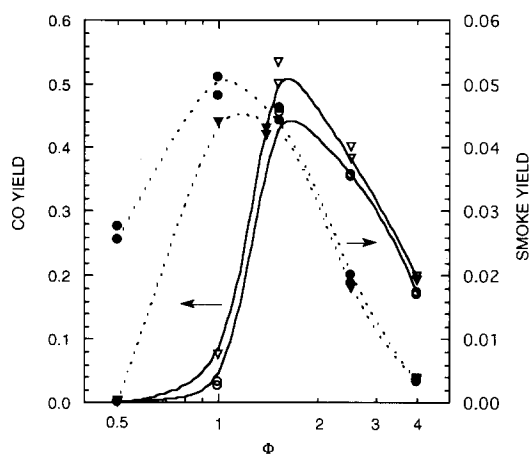


Fig. 10. Yield of CO (burner configuration 1, O; burner configuration 2, ▽) and smoke (burner configuration 1, ●; burner configuration 2, ▼) for ethene at a fuel flow rate of $6.4 \text{ cm}^3/\text{s}$.

TABLE 3
Organic and Elemental Carbon Analysis

Methane 10 cm ³ /s					
Φ	Organic Carbon ($\mu\text{g}/\text{cm}^2$)	Organic Carbon Error	Elemental Carbon ($\mu\text{g}/\text{cm}^2$)	Elemental Carbon Error	Organic/Elemental
1	1.0	0.2	21	1	0.05
2	8.4	0.5	4.9	0.3	1.7
4	3.4	0.3	0.4	0.1	8.5
4	5.2	0.4	1.0	0.2	5.2
Ethene 6.4 cm ³ /s					
0.50	0.7	0.1	19	1	0.04
1	1.3	0.2	27	1	0.05
2	7.2	0.5	15	0.9	0.48
4	7.0	0.5	6.2	0.4	1.13

Additional evidence of the difference in character of the high Φ smoke compared with the low Φ smoke are the electron micrographs (Fig. 11) of the ethene smoke collected at $\Phi = 4$ and $\Phi = 1$. We see that while in both cases the smoke has an agglomerated structure, at $\Phi = 4$ the agglomerate is agglutinated indicating the presence of a liquidlike component. A Phillips 420T transmission electron

microscope was used at a voltage of 100 kV with a 60,000 \times magnification to obtain the images shown in Fig. 11.

DISCUSSION

The discussion is focused on the results for underventilated burning, but our new finding for overventilated burning that increasing the

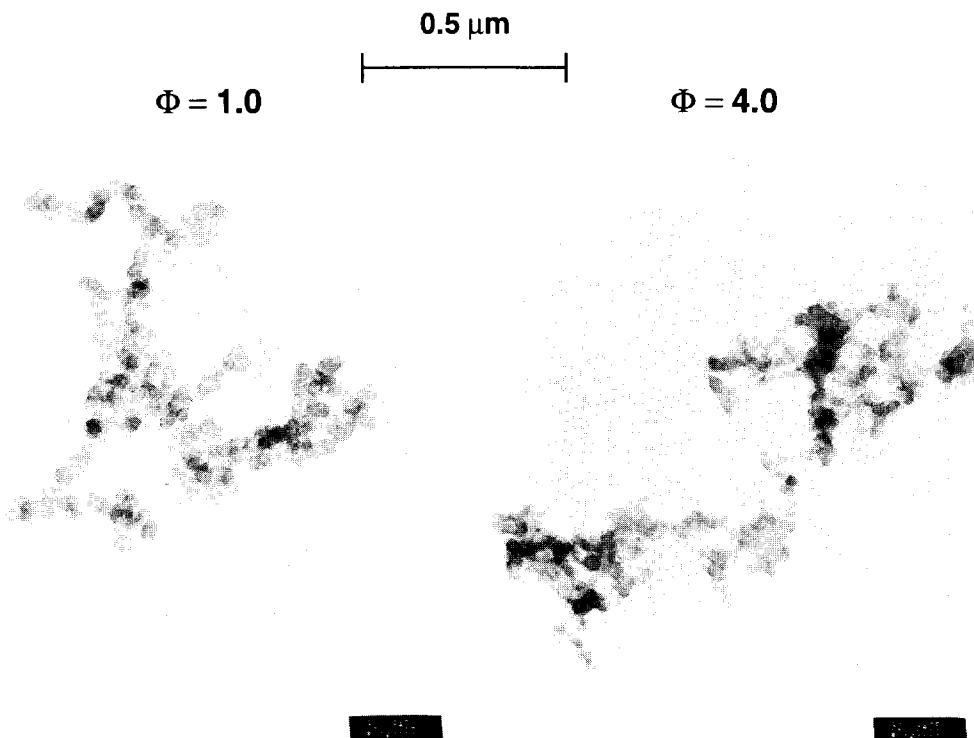


Fig. 11. TEM photographs of smoke collected from an ethene flame at $\Phi = 1$ (left) and at $\Phi = 4$ (right).

velocity of air relative to the fuel velocity changes a smoking ethene diffusion flame to a nonsmoking flame invites notice.

The peak CO yields for methane and ethene differ by only 20%, while the peak smoke yields differ by about a factor of five. The result that CO yield is insensitive to fuel structure while smoke yield is affected by fuel structure for underventilated laminar diffusion flames differs markedly from the approximate proportionality between CO and smoke yields for overventilated turbulent diffusion flames observed by Köylü et al. [25] for gaseous hydrocarbon fuels and Mulholland et al. [26] for plastics and Douglas fir as well as by several other workers for a variety of fire related studies [5, 27, 28].

One difficulty with the definitions of CO and smoke yields given by Eqs. 5 and 6 is that as Φ increases much of the fuel is not involved in the reaction. A better normalization in regard to analyzing chemical effects is the CO yield per gram of fuel consumed or per gram of oxygen consumed. Here we compute the yield based on oxygen consumption because the data analysis is simpler in this case. For $\Phi \geq 1$, the oxygen consumed is estimated from the inlet flow rate of oxygen. Subsequent measurements using GC analysis demonstrated that this was a reasonable approximation. It was found that the exit flow of oxygen was 8%–14% of the inlet oxygen flow for $\Phi = 4$ and 3%–6% of the inlet oxygen flow for $\Phi = 1.52$ and 2.52. For $\Phi < 1$, we compute the mass flow rate of oxygen consumed from the mass flow rate of fuel times the mass of oxygen required to completely burn a unit mass of fuel (4.00 for methane and 3.43 for ethene). This is a good approximation, since CO_2 and water account for at least 95% of the combustion products for fuel lean burning. As shown in Fig. 12, the CO yield per gram O_2 consumed varies much less for $\Phi > 1.5$ compared with the CO yield per gram fuel entering the burner as shown in Fig. 7. The ratio of the maximum to the minimum yield of CO over the Φ range, $1.5 < \Phi < 4$, is 1.3 per gram O_2 consumed and 2.6 per gram of fuel entering the burner.

It is also of interest to consider local measurements for laminar methane flames for overventilated burning by Mitchell et al. [14]

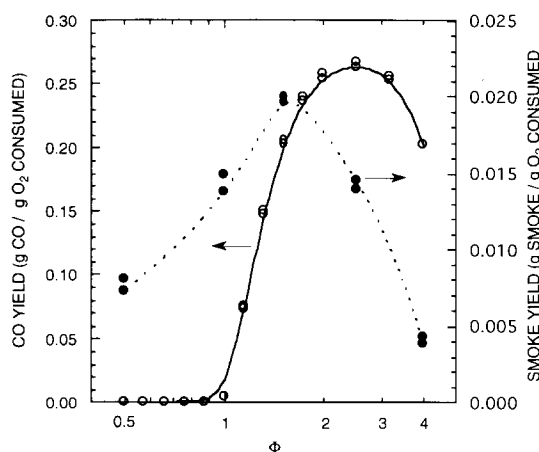


Fig. 12. Yield of CO (○) and smoke (●) per g of oxygen consumed for ethene at a fuel flow rate of $6.4 \text{ cm}^3/\text{s}$.

and for underventilated burning by Puri [29] to obtain insight regarding our result of a nearly constant CO yield per gram O_2 . The comparison will be made in terms of the ratio of the volume percent of CO to the volume percent of CO_2 , since not all the data needed for computing yield are available. This ratio is a useful parameter for assessing changes in flame chemistry, since CO and CO_2 comprise the major carbon containing products of combustion. The ratio $X_{\text{CO}}/X_{\text{CO}_2}$ obtained in each of these studies is relatively constant with a value of 0.6 over the local equivalence ratio range $1.5 < \Phi < 4$ as shown in Fig. 13. It is also seen in Fig. 13 that our global measurements are qualitatively similar to the local measurements but with a lower peak ratio of about 0.43 compared with 0.6 and with a slight decrease with increasing Φ . The uncertainty in the ratio is estimated as $\pm 5\%$ of the measured ratio based on the uncertainty in the gas analyzer readings and the experimental repeatability. The local measurements indicate that the CO and CO_2 are unreactive for $\Phi > 1.5$ presumably because of the lack of oxygen and the decrease in temperature. Abam [30] has also reported that the methane flame is unreactive for large Φ . It is not surprising that our global measurement of $X_{\text{CO}}/X_{\text{CO}_2}$ is less than the local $X_{\text{CO}}/X_{\text{CO}_2}$, since some of the CO production locally takes place under fuel lean conditions for which the CO yield is low.

As mentioned in the Introduction, measurements have been made on the CO and CO_2

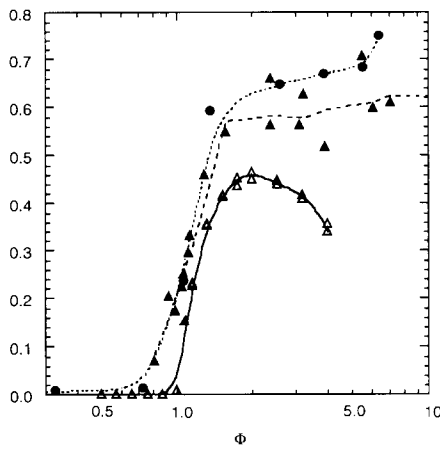


Fig. 13. Local ratio X_{CO}/X_{CO_2} versus local equivalence ratio for overventilated methane flame (\bullet), for underventilated methane flame (\blacktriangle), and global ratio X_{CO}/X_{CO_2} versus global equivalence ratio for underventilated methane flame (\triangle , this study with either 2 or 4 repeat measurements for each value of Φ).

concentrations [6–10] versus the global equivalence ratio for turbulent natural gas flames, which were typically 94% methane. In these experiments [6–10] the air entrainment into the flame was controlled by adjusting the height of the collection hood relative to the burner. As shown in Fig. 14, the ratio X_{CO}/X_{CO_2} for our study with the laminar methane flame increases much more abruptly with Φ near $\Phi = 1$ compared to the ratio for the turbulent natu-

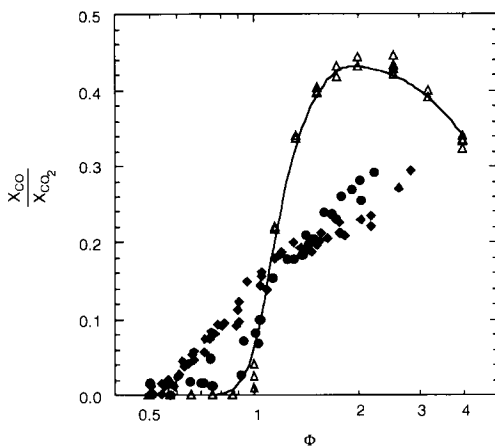


Fig. 14. X_{CO}/X_{CO_2} versus Φ for laminar burning of methane at a fuel flow rate of $10 \text{ cm}^3/\text{s}$ (\triangle this study with either 2 or 4 repeat measurements for each value of Φ) and for turbulent burning of natural gas (\bullet , Ref. 4, \blacklozenge , Ref. 5).

ral gas study [6, 7]. Also, the ratio X_{CO}/X_{CO_2} is larger for the laminar burner results for $\Phi > 1$; for example, at $\Phi = 2$, the ratio is 0.43 compared with 0.24 for the turbulent flame.

The effect of Φ on smoke is more complex than for CO, because not only the yield changes but also the soot chemical makeup varies. The decreasing yield of smoke with increasing Φ indicated in Fig. 12 may be a result of the smaller flame height and consequently shorter residence time for smoke particle growth. The much longer reaction time needed for the formation and growth of smoke particles compared to the formation of CO and CO_2 may also be responsible for the peak in smoke yield occurring at a smaller Φ , which means greater flame height and longer residence time, compared with CO.

As Φ increases, the organic content of the smoke increases and electron microscopy indicates that the smoke agglomerates change from clusters of distinct particles to agglutinated structures with more apparent liquid character. Previous studies on the organic content of smoke have been for highly overventilated conditions where the object is burning in the open. Under these conditions for large-scale tests, the organic fraction of the smoke was found to be at most 25% for the burning of crude oil, lumber, plywood, heptane, polyurethane, and asphalt shingles [31–33]. Our results are the first to show that more than 50% of the smoke produced from flaming combustion of a hydrocarbon fuel can be organic. In fact, for methane, 80%–90% of the smoke is organic for $\Phi = 4$.

It is intriguing to speculate that the high organic content at high equivalence ratio results from the quenching of the smoke growth at an early stage because of the small flame height (Fig. 3). That is, there may be a chemical similarity between this smoke and the incipient smoke in a laminar overventilated diffusion flame. Dobbins et al. [34] have reported agglutinated structures of young aggregates when sampling low in a diffusion flame.

SUMMARY

An investigation of the generation of CO and smoke for underventilated laminar diffusion

flames, burning methane and ethene, has revealed differences with studies considering turbulent overventilated conditions. In particular, the proportionality between smoke yield and CO yield observed for the postflame (overfire) region of turbulent overventilated flames for a wide range of fuels is not found to be valid for the underventilated laminar diffusion flame case. In fact, the soot observed in the underventilated flames is observed to vary considerably in terms of the chemical structure from that typically observed in overventilated flames. The highly organic nature of the soot implies that the structure of the soot may be more similar to early agglutinated soot particles recently observed in diffusion flames than to the more aged aggregates typical of the postflame region for overventilated flames. Comparisons in terms of the ratio of CO and CO₂ as a function of global equivalence ratio in the postflame region of the underventilated flames show a similar behavior to that previously observed for in-flame measurements for both overventilated and underventilated diffusion flames that examined the dependence of this ratio on local equivalence ratio conditions. This suggests that for the in-flame fuel-rich region, the chemical environment excluding soot is correlated with equivalence ratio in a similar way for both an overventilated flame and an underventilated flame. The low production of CO in the postflame region of overventilated flames is simply a result of the oxidation of CO to CO₂ in the upper regions of these flames. Finally, the present studies illustrate the utility of the study of underventilated flame environments where product yields and trends can be quite different from overventilated conditions. These studies should have significance for combustion phenomena in which underventilated conditions are typical, such as in fires.

The support of this work by the National Institute of Standards and Technology under Grant 60NANB0D1035 is gratefully acknowledged. One of the authors (GWM) was supported in part by The Pennsylvania State University Particulate Materials Center while on sabbatical leave at Penn State. The authors would also like to thank Mr. Daniel Boone for his able assistance in the construction of the experimental apparatus.

REFERENCES

- Burke, S. P., and Schumann, T. E. W., *Ind. Eng. Chem.*, 20:998-1004 (1928).
- Wu, K-T., and Essenhigh, R. H., *Twentieth Symposium (International) on Combustion*, The Combustion Institute, Pittsburgh, 1984, pp. 1925-1932.
- Sidebotham, G. W., and Glassman, I., *Combust. Flame* 90:269-283 (1992).
- Tewarson, A., and Steciak, J., *Combust. Flame* 53:123-134 (1983).
- Tewarson, A., in *The SFPE Handbook of Fire Protection Engineering* (P. DiNenno, C. Beyler, R. Custer, W. Walton, and J. Watts, Jr., Eds.), National Fire Protection Assoc., Quincy, MA., (1988), pp. 1-179 to 1-199.
- Toner, S. J., Zukoski, E. E., and Kubota, T., National Bureau of Standards—Grant Contract Research Report 87-528, Gaithersburg, MD (1987).
- Morehart, J. H., Zukoski, E. E., and Kubota, T., National Institute of Standards and Technology—Grants Contract Research Report 90-585, Gaithersburg, MD (1990).
- Zukoski, E. E., Morehart, J. H., Kubota, T., and Toner, S. J., *Combust. Flame* 83:325-332 (1991).
- Zukoski, E. E., Toner, S. J., Morehart, J. H., and Kubota, T., in *Proceedings of the Second Fire Safety Science International Symposium*, (T. Wakamatsu, Y. Hasemi, A. Sekizawa, P. G. Seeger, P. J. Pagni, and C. E. Grant, Eds.), 1989, pp. 295-304.
- Beyler, C. L., *Fire Safety J.* 10:47-56 (1986).
- Beyler, C. L., in *Proceedings of the First Fire Safety Science International Symposium* (C. Grant and P. Pagni, Eds.), Hemisphere, New York, 1986, pp. 431-440.
- Gottuk, D. T., Roby, R. J., Peatross, M. J., and Beyler, C. L., *J. Fire Prot. Eng.* 4:133-150 (1992).
- Bryner, N. P., Johnsson, R. L., and Pitts, W. M., "Carbon Monoxide Production in Compartment Fires—Reduced Scale Test Facility," National Institute of Standards and Technology, Internal Report, Gaithersburg, MD, to appear.
- Mitchell, R. E., Sarofim, A. F., and Clomburg, L. A., *Combust. Flame* 37:227-244 (1980).
- Smyth, K. C., Miller, J. H., Dorfman, R. C., Mallard, W. G., and Santoro, R. J., *Combust. Flame* 62:157-181 (1985).
- Garro, A., Lahaye, J., and Prado, G., *Twenty-First Symposium (International) on Combustion*, The Combustion Institute, Pittsburgh, 1986, pp. 1023-1031.
- Garro, A., Prado, G., and Lahaye, J., *Combust. Flame* 79:226-233 (1990).
- Kent, J. H., and Wagner, H. Gg., *Combust. Sci. Technol.* 41:245-269 (1984).
- Santoro, R. J., Semerjian, H. G., and Dobbins, R. A., *Combust. Flame* 51:203-218 (1983).
- Honnery, D. R., and Kent, J. H., *Combust. Flame* 82:426-434 (1990).
- Santoro, R. J., Yeh, T. T., Horvath, J. J., and Semerjian, H. G., *Combust. Sci. Technol.* 53:89-115 (1987).

22. Liu, B. Y. H., Pui, D. Y. H., and Rubow, K. L., in *Aerosol in the Mining and Industrial Work Environment* (V. A. Marple and B. Y. H. Liu, Eds.), Elsevier, Amsterdam, 1983, Vol. 3, p. 989.
23. Johnson, R. L., Shah, J. J., Cary, R. A., and Huntzicker, J. J., *Atmospheric Aerosol: Source/Air Quality Relationships*, ACS Symposium Series 167, American Chemical Society, Washington, D.C., 1981.
24. Roper, F. G., Smith, C., and Cunningham, A. C., *Combust. Flame* 29:227-234 (1977).
25. Köylü, Ü. Ö., Sivathanu, Y. R., and Faeth, G. M., in *Proceedings of the Third Fire Safety Science International Symposium* (G. Cox and B. Langford, Eds.), Elsevier, 1991, pp. 625-634.
26. Mulholland, G., Yusa, S., Yanssens, M., Twilley, W., and Babrauskas, V., in *Proceedings of the Third Fire Safety Science International Symposium* (G. Cox and B. Langford, Eds.), Elsevier, 1991, pp. 585-594.
27. McCaffrey, B. J., and Harkleroad, M., *Twenty-Second Symposium (International) on Combustion*, The Combustion Institute, Pittsburgh, 1988, pp. 1251-1261.
28. Friedman, R., *Proceedings of the First International Symposium on Fire Safety Science* (C. Grant and P. Pagni, Eds.), Hemisphere, New York, 1986, pp. 349-359.
29. Puri, R., Ph.D. thesis, The Pennsylvania State University (1992).
30. Abam, D. P. S., *Combust. Flame* 68:95-107 (1987).
31. Mulholland, G. W., Henzel, V., and Babrauskas, V., in *Proceedings of the Second Fire Safety Science International Symposium* (T. Wakamatsu, Y. Hasemi, A. Sekizawa, P. G. Seeger, P. J. Pagni, and C. E. Grant, Eds.), 1989, pp. 347-357.
32. Benner, B. A., Bryner, N. P., Wise, S. A., and Mulholland, G. W., *Envir. Sci. and Tech.*, 24:1418-1427 (1990).
33. Dod, R. L., Brown, N. J., Mowrer, F. W., Novakov, T., and Williamson, R. B., *Aerosol Sci. Tech.* 10:20-27 (1989).
34. Dobbins, R. A. and Subramaniasivam, H. Heidelberg Conference entitled "Presentations on Mechanisms and Models of Soot Formation, Heidelberg Conference", October 1991, to appear in *Lecture Notes in Physics*, Springer-Verlag.

Received 27 May 1993; revised 23 November 1993